



HAL
open science

Changes in mineralogy and microstructure of a lime-treated silty soil during curing time

Zi Ying, Yu-Jun Cui, Nadia Benahmed, Myriam Duc

► To cite this version:

Zi Ying, Yu-Jun Cui, Nadia Benahmed, Myriam Duc. Changes in mineralogy and microstructure of a lime-treated silty soil during curing time. E3S Web of Conferences, 2020, pp.1-6/03044. <10.1051/e3sconf/202019503044>. <hal-03620143>

HAL Id: hal-03620143

<https://hal.inrae.fr/hal-03620143v1>

Submitted on 5 Dec 2023

HAL is a multi-disciplinary open access archive for the deposit and dissemination of scientific research documents, whether they are published or not. The documents may come from teaching and research institutions in France or abroad, or from public or private research centers.

L'archive ouverte pluridisciplinaire HAL, est destinée au dépôt et à la diffusion de documents scientifiques de niveau recherche, publiés ou non, émanant des établissements d'enseignement et de recherche français ou étrangers, des laboratoires publics ou privés.



Distributed under a Creative Commons CC BY 4.0 - Attribution - International License

Changes in mineralogy and microstructure of a lime-treated silty soil during curing time

Zi YING¹, Yu-jun Cui^{1,*}, Nadia Benahmed², and Myriam Duc³

¹Ecole des Ponts ParisTech, Laboratoire Navier/CERMES, 6-8 av. Blaise Pascal, Cité Descartes, Champs-sur-Marne, 77455 Marne-la-Vallée cedex 2, France

²Irstea, Aix Marseille Univ, RECOVER, Equipe G2DR, 3275 route Cézanne, CS 40061, 13182 Aix-en-Provence, France

³Université Paris Est, IFSTTAR/GERS/SRO, 14-20 boulevard Newton, Champs-sur-Marne, 77447 Marne-la-Vallée, France

Abstract. Lime treatment is widely applied to improve the workability and long-term durability of soils. In this study, the curing time effect on the mineralogy and microstructure of lime-treated soil was investigated. The soil samples were prepared with 2 % lime and statically compacted at dry ($w = 17\%$) and wet ($w = 20\%$) sides of optimum. X-ray diffraction (XRD) and mercury intrusion porosimetry (MIP) were performed on lime-treated soil at various curing times. The presence of XRD peaks attributed to portlandite even after 150 days curing time indicated that it was not totally converted in cementitious compounds after reaction with silica and alumina from clay minerals. By contrast, no obvious XRD reflections of well-crystallized cementitious compounds were identified. Furthermore, all samples compacted at dry and wet side of optimum exhibited bi-modal pore size distribution, with a decrease of macro-pore frequency with increasing water content. The microstructure changes with increasing curing time did not follow monotonic tendency. On the whole, the quantities of pores less than $0.006\ \mu\text{m}$ and micro-pores increased and the quantity of macro-pores decreased with increasing curing time due to the possible creation of poorly crystallized or amorphous cementitious compounds.

1 Introduction

Lime stabilization is a widespread technique applied in recent years to soils with poor physical and mechanical characteristics. Lime can significantly improve soil hydro-mechanical behaviour owing to series of physical-chemical reactions, including lime hydration, cation exchange and pozzolanic reaction [1-3]. The cementitious compounds produced in pozzolanic reaction play a major role in improving soil hydro-mechanical behaviour [3-4].

The production of cementitious compounds is strongly dependent on curing time and mineral composition of soils. For the lime-treated Impersol soil which contained 86 % clay minerals (48 % bentonite and 38 % kaolinite), the products from pozzolanic reaction were observed in the form of calcium aluminate hydrate (C-A-H) after 1 day and in the form of calcium silicate hydrate (C-S-H) after 7 days of curing [5]. The C-S-H phase was detected for lime-treated silty soil with 27 % clay-size fraction after 1 year curing [6]. Finally, the formation of C-S-H was identified for lime-treated quartz SiO₂ [1]. Indeed, the cementitious compounds were not only produced from the reactions of lime and alumino-silicate such as clay minerals but also from the reactions of lime and silicate such as fine quartz (or feldspars). The presence of a low amount of amorphous silica mixed with quartz and characterized by higher

dissolution ability than well crystallized quartz may explain such result. Note that the carbonation of lime hydration products were usually put aside considering that the soil was under compacted form prevented in major case from air contact.

Microstructure changes of lime-treated soil were also analysed in several studies. Lemaire et al. [7] reported that for lime-treated silty soil, the cementitious compounds produced by the pozzolanic reaction were distributed continuously around the agglomerates which were constituted by clay and large-sized quartz particles. They pointed out that the pores within these agglomerates were identified as micro-pores and the pores between agglomerates were regarded as macro-pores. Lime addition caused the creation of smaller pores due to the formation of cementitious compounds [6-9]. Indeed, the cementitious compounds gradually coated the surface of soil aggregates and bonded the soil particles together, leading to a reduction of the modal sizes and the frequencies of micro-pores and macro-pores. As these cementitious compounds filled the pores and blocked some entrances of micro-pores, the total intrusion value decreased with curing time [6, 10-11].

The above studies highlighted the mineralogy and microstructure evolutions of lime-treated soil with curing time. However, few studies have been focused on lime-treated silty soil with low amount of clay. In this study, the changes of mineralogy and microstructure of lime-

* Corresponding author: yu-jun.cui@enpc.fr

treated silty soil during curing time were analysed. Two groups of samples were prepared at dry and wet sides of optimum. X-ray diffraction (XRD) and mercury intrusion porosimetry (MIP) were carried out to investigate the mineral composition and the pore size distribution of lime-treated soil.

2 Materials and methods

The tested soil was taken from Salin-de-Giraud, a traditional salt exploitation site in France. Its geotechnical properties are reported in Table 1. The natural soil was air-dried, gently ground and passed through the 0.4 mm sieve. The grain size and aggregate size distribution of natural soil and dry sieved soil powder are presented in Fig. 1. The natural soil was composed of 63 % silt particles (0.002 ~ 0.075 mm) while the dry soil powder mainly consisted of 62 % sand particles (0.075 ~ 2 mm). The soil salinity, defined as the mass ratio of salt to dry soil, was 2.1 ‰ (g of salt/ kg of dry soil).

Table 1. Geotechnical properties of the tested soil

Property	Value
Specific gravity, G_s	2.71
Liquid limit, w_L (%)	29
Plastic limit, w_p (%)	19
Plasticity Index, I_p	10
VBS (g/100g)	0.98
Specif. surf. Area, SSA(m^2/g)	24.0

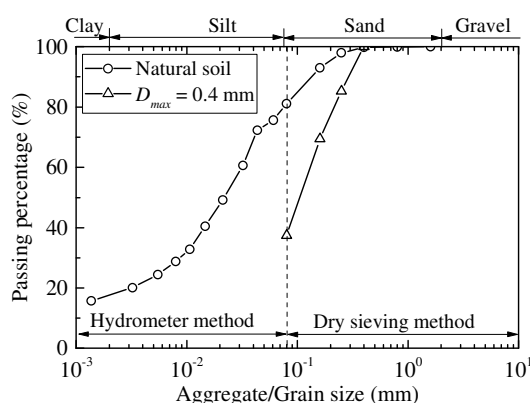


Fig. 1. Aggregate/Grain size distribution of dry sieved soil ($D_{max} = 0.4$ mm) and natural soil.

Dry soil powder and 2 % quicklime (by weight of dry soil) were mixed thoroughly. Then, the soil-lime mixture was humidified by spraying deionized water to reach different target water contents. After mellowing for 1 h, static compaction was performed to prepare samples at the target dry density. Both dry ($w = 17$ %) and wet sides ($w = 20$ %) of optimum water content with the same dry density ($\rho_d = 1.63$ Mg/m³) were considered, according

to the normal proctor compaction curve of 2 % lime-treated soil presented in Fig. 2. After compaction, the samples were wrapped and cured at different times. At a given curing time, the samples were freeze-dried following the procedure proposed by Delage and Pellerin [12].

X-ray diffraction (XRD) analysis was performed on both untreated and lime-treated soil for mineralogy investigation. The freeze-dried samples were first crushed to pass entirely through 80 μm sieve prior to XRD analysis. Samples were loaded into XRD sample holder by sprinkling the powder through a 200 μm sieve. Then, the superfluous soil was removed by cutting the surface with a thin razor blade that prevented the particles from preferential orientation. XRD patterns were collected with a D8 Advance diffractometer (from Bruker) equipped with Cobalt anode, no monochromator, and a lynx eye rapid detector (acquisition during 1s per 0.01° 2theta). Minerals were identified with EVA software coupled with ICDDPDF2 database and the quantification was established with TOPAS software.

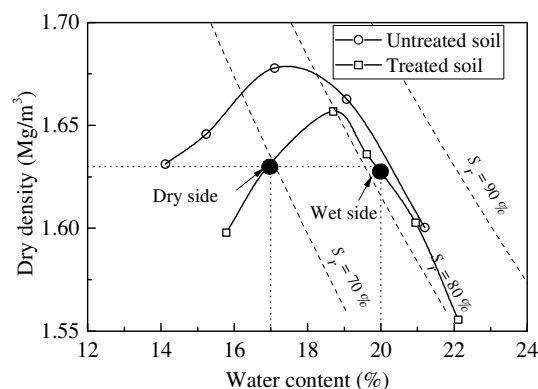


Fig. 2. Normal proctor curve of untreated and 2 % lime-treated soil.

Autopore IV 9500 mercury intrusion porosimeter (from Micromeritics) was used to investigate the microstructure of lime-treated soil. The applied pressure ranged from 3.6 kPa to 230 MPa, and the corresponding intruded diameter varied from 0.006 μm to 350 μm . According to the MIP results, the delimiting diameter between micro-pores and macro-pores can be determined following the method proposed by Zhang et al. [13]. This method based on the water retention curve deduced from MIP results and the soil suction considering the higher sensitivity of micro-pores than macro-pores as water content changed.

3 Results

3.1. Mineralogical analysis

Fig. 3a shows the XRD patterns of the untreated soil and lime-treated soil compacted on dry side. Note that mineralogical analysis was only conducted on dry samples. Measurement on wet side should confirm similar mineralogy. The main minerals of untreated soil

were found to be quartz (39 %), calcite (35 %) and clay (15.7 %) with small amount of feldspars (9.5 %) and halite NaCl (0.8 %). The clay compositions were identified as illite (10.8 %), chlorite (3.6 %) and kaolinite (1.3 %) and the whole content (15.7 %) was consistent with the clay-size fraction (< 2 μm) estimated at 17.4 % on Fig 1. These clay minerals were also present in the lime-treated soil and no clear changes in their content were measured even after 150 days. To better identify the mineralogy changes for lime-treated soil during curing, the XRD patterns between 20° to 25° (2θ) and 32° to 41° (2θ) are depicted in Fig. 3b and 3c. For the lime-treated soil at curing time of 1, 90 and 150 days, three new reflections at 2θ equal to 21.0° (d ~ 4.90 Å), 33.4° (d ~ 3.09 Å) and 39.8° (d ~ 2.63 Å) were identified, suggesting the appearance of portlandite. The portlandite, namely calcium hydroxide Ca(OH)₂, was produced immediately when soil, lime and water were mixed together. Calcium hydroxide provided an alkaline environment in soil, inducing the dissolution of the silica and alumina present in the clay minerals. Then, the released Si and Al may react with Ca from the Ca(OH)₂ and form cementitious compounds [4-5]. However, the portlandite XRD reflections were still observed after 150-day curing, suggesting that the portlandite consumption was not complete and might extend longer. Furthermore, following the observations by Wang et al. [6], a reflection corresponding to cementitious compounds at 2θ equal to 34.2° (d ~ 3.04 Å) was identified for a lime-treated soil after 1-year curing. However, for the tested soil in this study, the reflection at 34.2° 2θ was occupied by the main XRD peak of calcite, as shown in Fig. 3a. A small heave around the reflection at 34.2° 2θ may be associated with the formation of poorly crystallized or amorphous cementitious compounds (Fig. 3c).

3.2 Pore size distribution

The cumulative curves and the corresponding derived curves of lime-treated samples compacted on dry and wet sides of optimum are presented in Fig. 4 and in Fig. 5, respectively. With increasing curing time, the total intruded void ratio for dry samples decreased from 0.64 at 1 day curing to 0.59 at 28 days, whereas the total intruded void ratio for samples at 90 days was slightly larger than the sample at 1 day curing (Fig. 4a). The total intruded void ratio for the wet samples at 90 days was smaller than for the sample at 1 day. However, for the samples at 7 days and 28 days, it was slightly larger than for the samples at 1-day curing (Fig. 5a).

The pore size distribution of lime-treated samples compacted on both dry and wet sides of optimum presented bi-modal characteristics, with a population of macro-pores and a population of micro-pores. The frequency of macro-pores decreased with increasing water content. The microstructure changes for the lime-treated samples with increasing curing time did not follow a monotonic tendency. For the dry samples (Fig. 4b), the modal size of micro-pores decreased from 0.89 μm to 0.63 μm after 90-day curing while for the

population of macro-pores, its modal size decreased from 7.50 μm after 1-day curing to 4.99 μm after 28-day curing, then increased to 7.00 μm at 90-day curing. As for the samples compacted on wet side (Fig. 5b), the modal size of micro-pores was around 1.04 μm for all samples at different curing times. The modal size of macro-pores decreased from 5.63 μm at 1-day curing to 5.00 μm after 90-day curing, whereas the modal sizes of macro-pores for samples at 7 days and 28 days were larger than those of samples at curing time of 1 day and 90 days.

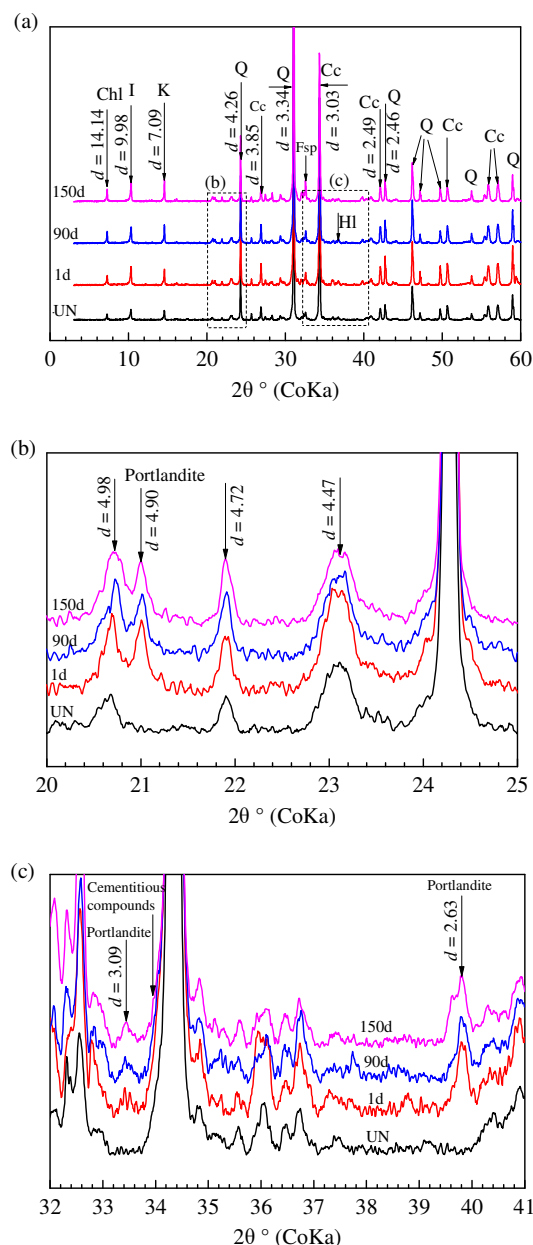


Fig. 3. X-ray diffraction patterns of untreated and lime-treated samples compacted on dry side: (a) 2θ 0°-60°; (b) 2θ 20°-25°; (c) 2θ 32°-41° (UN: untreated; Chl: chlorite; I: illite; K: kaolinite; Q: quartz; Cc: calcite; Fsp: feldspar; HI: halite).

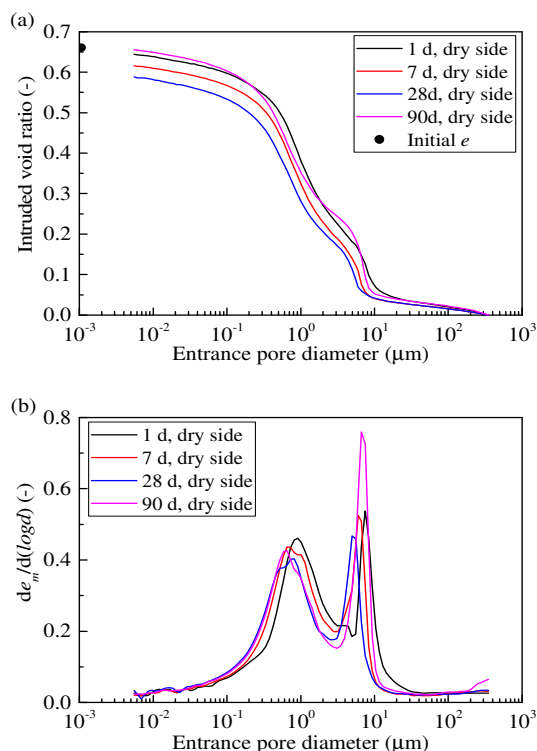


Fig. 4. MIP results of samples compacted on dry side: (a) cumulative curves, (b) derived curves.

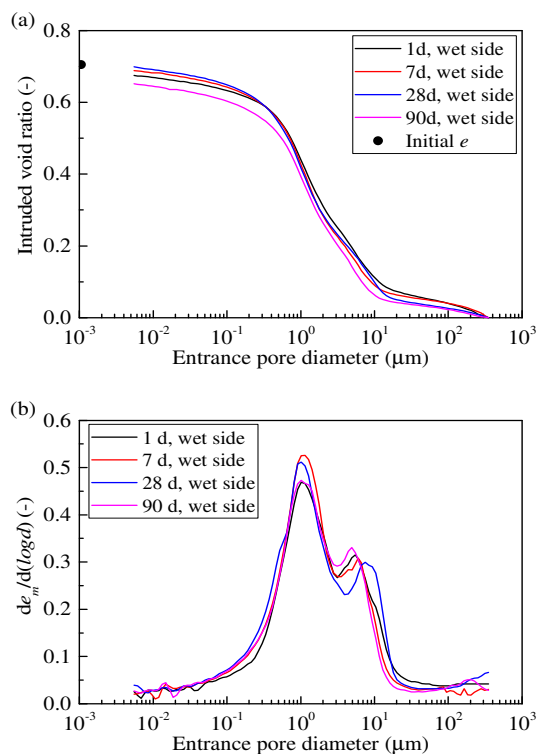


Fig. 5. MIP results of samples compacted on wet side: (a) cumulative curves, (b) derived curves.

To better distinguish the change tendency of the microstructure for lime-treated soil during curing time, the quantity of each pore population was given as the ratio of intruded void ratio to the initial void ratio which was calculated from the global parameters of compacted samples, as illustrated in Table 2. Note that the void ratio

of pores $< 0.006 \mu\text{m}$ was not quantified by porosimeter but its value was estimated by the value of initial void ratio minus the total mercury intruded void ratio. If the total intruded void ratio was larger than the initial value, the void ratio of pores $< 0.006 \mu\text{m}$ was regarded as zero. On the whole, the quantities of pores $< 0.006 \mu\text{m}$ and micro-pores increased, whereas the quantity of macro-pores decreased with curing time, except for the dry sample at 90 days.

Table 2. Quantity of the different pore populations.

Samples	Delimiting diameter $d_L(\mu\text{m})$	Pores $< 0.006 \mu\text{m}$ (%)	Micro-pores	Macro-pores	
			$0.006 \mu\text{m} - d_L(\%)$	$> d_L(\%)$	
Dry side	1 d	1.32	2.7	47.2	50.1
	7 d	1.16	7.1	58.2	34.7
	28 d	1.05	11.2	54.8	34
	90 d	1.03	1.1	46	52.9
Wet side	1 d	1.66	0	49.1	50.9
	7 d	1.57	0	51	49
	28 d	1.57	0	51.6	48.4
	90 d	1.59	2.7	52.3	45

4 Discussions

XRD patterns of lime-treated soil showed new peaks at $\sim 4.90 \text{ \AA}$, $\sim 3.09 \text{ \AA}$ and $\sim 2.63 \text{ \AA}$ corresponding to portlandite produced during lime hydration process. The presence of remaining portlandite in lime-treated soil after 150-day curing indicated that the lime was not consumed completely. This can be explained both by the slow pozzolanic process and by the low clay fraction present in the tested soil. Low water content in dry or wet soil was in favour of low portlandite dissolution in soil pore water, followed by diffusion. Then, the low amount of clay, especially clay with low ability to dissolve such as illite and chlorite, cannot provide enough activated silica and alumina in order to interact with calcium and form cementitious compound. Other phases present in soil such as quartz and feldspars could also contribute but their usual low ability to dissolve compared to clay one, limited their role in pozzolanic reaction. Furthermore, as for a silty soil, the clay coated the granular quartz grains to constitute agglomerates and lime powder was solely distributed at the surface of these agglomerates without penetrating them [7, 14]. Therefore, the lime could preferentially react with soluble silica and alumina in clay minerals but not with the inert quartz minerals.

Concerning the cementitious compounds, the lack of XRD observations was usually attributed to the absence of well-crystallized cementitious compounds [6, 15]. Besides, the high intensity of natural calcite on XRD patterns may also mask the potential reflections of cementitious compounds (Fig. 3c).

Considering the pore size distribution of lime-treated soil, the curing time effect was consistent with the

mineralogical analysis. The insignificant microstructure changes with increasing curing time did correspond to the formation of a low quantity of cementitious compounds probably in poorly crystallized or amorphous form. On the whole, the quantity of pores $< 0.006 \mu\text{m}$ and micro-pores for samples compacted on wet and dry sides increased, and the quantity of macro-pores decreased with curing time. The pores $< 0.006 \mu\text{m}$ were correlated with the formation of poorly crystallized or amorphous cementitious compounds produced in pozzolanic reaction, whose small internal pores were undetectable by MIP measurement due to the apparatus detection limit. This was in agreement with the observations made by Wang et al. [6]. Such new cementitious compounds gradually covered soil aggregates, and bonded adjacent soil particles together parallel to the filling of macropores. Then, it shifted the modal sizes to lower values, leading to a decrease of the quantity of macro-pores and an increase in the quantity of micro-pores [6-7, 10-11].

In general, the samples compacted on dry side exhibited aggregated structure with larger macro-pores and smaller micro-pores, while the samples compacted on wet side exhibited dispersed (or continuous) structure with only micro-pores [11, 16]. Thus, a bi-modal pore size distribution curves for wet samples as observed in this study was not a common result. However, Burton et al. [17] indicated that the bi-modal pore size distribution characteristics was not limited to samples compacted on dry side, but may also concern samples compacted on wet side if their compaction energy and degree of saturation were low. Delage et al. [16] indicated also that the volume of clay phase at equal dry density was an important parameter to understand the water content effect on compaction structure. On the dry side, the clay fraction was not well expanded and clays were coated on the surface of grains, leading to an aggregated structure characterized by populations of micro-pores and macro-pores. With increasing water content, the clay fraction formed a continuous or more compact matrix around the silt grains and clays were able to fill the macro-pores.

As for the lime-treated soil, the compacted dry density was estimated at 1.63 Mg/m^3 , close to the maximum dry density of 1.66 Mg/m^3 and the compacted water content was only 1.5 % larger than the optimum water content of 18.5 %. Thus, the compaction water content and the low clay fraction of the tested soil might be the possible reasons for the bi-modal pore size distribution identified on wet samples. The degree of saturation of wet samples was close to that at optimum state, but the compacted dry density was lower than the maximum dry density. Thus, wet samples at this compaction state preferentially exhibited bi-modal pore size distribution with a population of micro-pores and a small population of macro-pores, similar to the samples at optimum observed by Delage et al. [16]. Besides, the low fraction of clay paste surrounding partially silt grains, led to a decrease in the frequency of macro-pores but not eliminated them.

5 Conclusions

XRD and MIP tests were performed on lime-treated soil compacted at dry and wet sides of optimum. The curing time effect on mineralogy and microstructure of lime-treated soil was investigated. The obtained results allowed the following conclusions to be drawn:

- Portlandite observed on XRD pattern of lime-treated soil after curing time until 150 days, might be attributed to the limited water content in wet and dry samples combined with the low clay fraction that couldn't provide sufficient silica and alumina to interact with calcium from portlandite. Furthermore, no cementitious compounds in significant quantity were detected on XRD patterns even after a curing time as long as 150 days. The high intensity of calcite peak overlapping the reflection of hydrated products may explain such result. The formation of low amount of poorly crystallized or amorphous cementitious compounds might be the other possibility.

- The insignificant microstructure changes with increasing curing time were consistent with the formation of poorly crystallized or amorphous cementitious compounds whose pores were smaller than $0.006 \mu\text{m}$ and the quantity of these pores increased with curing time. Cementitious compounds gradually coated soil particles and bonded them together parallel to the filling of macropores, leading to a decrease of the quantity of macro-pores and an increase of the quantity of micro-pores.

- The samples compacted on dry and wet sides of optimum exhibited bi-modal pore size distribution characteristics with two populations of micro-pores and macro-pores. The smaller frequency of macro-pores for wet samples can be attributed to the slightly higher water content than optimum and the low clay fraction. The limited amount of clay paste surrounding the silt particles led to a decrease of the quantity of macro-pores but it did not eliminate them.

Acknowledgements

The authors would like to thank the China Scholarship Council (CSC), Ecole des Ponts ParisTech and IRSTEA for their financial support.

References

1. F. G. Bell, Eng. Geol., **42**, 223-237 (1996)
2. A. M. Tang, M. N. Vu, Y. J. Cui, Géotechnique, **61**, 421-429 (2011)
3. Y. J. Wang, Y. J. Cui, N. Benahmed, A. M. Tang, M. Duc, Géotechnique, 1-5 (2019)
4. Y. Guney, D. Sari, M. Cetin, M. Tuncan, Build. Environ., **42**, 681-688 (2007)
5. M. Al-Mukhtar, A. Lasledj, J. F. Alcover, Appl. Clay Sci., **50**, 191-198 (2010)
6. Y. J. Wang, M. Duc, Y. J. Cui, A. M. Tang, N. Benahmed, W. J. Sun, W. M. Ye, Appl. Clay Sci., **136**, 58-66 (2017)

7. K. Lemaire, D. Deneele, S. Bonnet, M. Legret, *Eng. Geol.*, **166**, 255-261 (2013)
8. O. Cuisinier, J. C. Auriol, T. L. Borgne, D. Deneele, *Eng. Geol.*, **123**, 187-193 (2011)
9. G. Russo, G. Modoni, *Géotechnique Lett.*, **3**, 93-97 (2013)
10. Y. J. Wang, Y. J. Cui, A. M. Tang, C. S. Tang, N. Benahmed, *Géotechnique Lett.*, **5**, 269-274 (2015)
11. Y. J. Wang, Y. J. Cui, A. M. Tang, C. S. Tang, N. Benahmed, *Eng. Geol.*, **202**, 114-121 (2016)
12. P. Delage, F. M. Pellerin, *Clay Miner.*, **19**, 151-160 (1984)
13. F. Zhang, Y. J. Cui, W. M. Ye, *Géotechnique Lett.*, **8**, 102-110 (2018)
14. B. Shi, Z. B. Liu, Y. Cai, X. P. Zhang, *J. Mater. Civ. Eng.*, **19**, 99-104 (2007)
15. M. Al-Mukhtar, A. Lasledj, J. F. Alcover, *Appl. Clay Sci.*, **95**, 133-145 (2014)
16. P. Delage, M. Audiguier, Y. J. Cui, M. D. Howat, *Can. Geotech. J.*, **33**, 150-158 (1996)
17. G. J. Burton, D. C. Sheng, C. Campbell, *Géotechnique Lett.*, **4**, 88-93 (2014)